Communications

Three-Dimensional Contour FDTD Modeling of Scattering from Single and Multiple Bodies

T. G. Jurgens and A. Taflove

Abstract—**This paper introduces a generalization of the three-dimensional finite difference time domain (FDTD) method, the three-dimensional contour FDTD (CFDTD) method. The FDTD method represents curved media boundaries as stepped edges. Through the use of subcell modeling, the CFDTD method conformably models bodies with curved surfaces, yet retains the ability to model corners and edges. Electromagnetic scattering from single and multiple bodies is presented.**

I. Introduction

The contour finite difference time domain (CFDTD) method is a generalization of the traditional finite difference time domain (FDTD) method [1]. One limitation of the FDTD method is its representation of curved media interfaces as a stair-stepped boundary. The analysis of the errors introduced by such an approximation have been analyzed elsewhere [2]. The CFDTD method allows the modeling of subcell geometries. Here three-dimensional (3-D) modeling of single and multiple body scattering is introduced. An earlier paper introduced the CFDTD modeling of two-dimensional (2-D) electromagnetic (EM) wave scattering from dielectric and metallic bodies [3]. The CFDTD method is applied to computational cells near a media interface, as opposed to nonorthogonal FDTD techniques which globally distort the mesh [4], [5]. Others have used the CFDTD method to study horn antennas [6], wave penetration through narrow slots and cracks [7], and thin dielectric structures [8]. In the field of accelerator physics, 2-D [9] and 3-D [10], [11] simulations using the CFDTD method have been used to study charged particle wake fields.

The discussion begins with a brief overview of the traditional FDTD method. Detailed descriptions and validations can be found elsewhere [12], [1]. The discussion then proceeds to the CFDTD finite difference equations and their relationship to the traditional FDTD equations. Next, validations are presented, and finally CFDTD computer resource needs are examined.

II. The Traditional FDTD Method

The traditional FDTD algorithm is a direct solution of a second order accurate finite difference approximation of Maxwell's time dependent curl equations:

$$\nabla \times \vec{H} = \frac{\partial \vec{D}}{\partial t} + \vec{J}_c + \vec{J}_s, \tag{1}$$

$$\nabla \times \vec{E} = -\frac{\partial \vec{B}}{\partial t}, \tag{2}$$

Manuscript received April 24, 1992; revised July 31, 1993.

T. G. Jurgens is with the Fermi National Accelerator Lab, Mail Stop 308, Batavia, IL 60510.

A. Taflove is with Northwestern University, Evanston, IL.

IEEE Log Number 9214094.

where $\vec{E}$, $\vec{D}$, $\vec{H}$, $\vec{B}$, $\vec{J}_c$, and $\vec{J}_s$ denote the electric field, electric flux density, magnetic field, magnetic flux density, conduction current, and source current, respectively. The constitutive relations are $\vec{D} = \epsilon\vec{E}$, $\vec{B} = \mu\vec{H}$, and $\vec{J}_c = \sigma\vec{E}$, where ϵ, μ, and σ are the medium's permittivity, permeability, and conductivity, respectively. The resulting difference equations are solved in a time-marching, leap-frog manner, with the alternate update of electric and magnetic field components. Examples of such equations can be found in [3].

The computations in the FDTD method are locally dependent. This allows different portions of the lattice to be computed on separate processors, underscoring the method's suitability for parallel processing. Because all the cells of the lattice are rectangular, this formulation models the curved surfaces of objects with a stair-step approximation.

The traditional FDTD code used in this investigation partitions the computational lattice into a total and scattered field region. The total field region completely contains all of the scattering bodies, while the scattered field region surrounds the total field region. A second-order accurate radiation boundary condition is applied at the lattice border permitting outward propagating waves to exit with minimal reflection [13]. Far fields are obtained using a near to far field transformation. Given the time evolution nature of this code, any waveform within the passband of the lattice can modeled [1].

III. The Contour FDTD Method

The CFDTD algorithm is a generalization of the FDTD algorithm. Rather than using Maxwell's curl equations, the CFDTD algorithm is based on Ampere's and Faraday's laws, shown below:

$$\oint_C \vec{H} \cdot d\vec{l} = \int\int_S \left(\vec{J}_c + \vec{J}_s\right) \cdot d\vec{S} + \frac{\partial}{\partial t} \int\int_S \vec{D} \cdot d\vec{S}, \tag{3}$$

$$\oint_C \vec{D} \cdot d\vec{l} = -\frac{\partial}{\partial t} \int\int_S \vec{B} \cdot d\vec{S}, \tag{4}$$

where the C contours enclose the S surfaces. Discretization of Ampere's and Faraday's laws result in difference equations which can be solved in a direct time marching manner that is similar to that used in the traditional FDTD method. In fact, the two methods employ identical difference equations for rectangular contours not near a media boundary. Near media boundaries the CFDTD method uses contours which allow subcell conformal modeling of the interface. The CFDTD method uses the traditional FDTD total field—scattered field lattice partition, near to far field transformation and radiation boundary condition since the contours are rectangular everywhere in the computational lattice except near media boundaries. The CFDTD method also inherits the FDTD code's ability to model time domain waveforms. The remainder of this section will discuss the modeling of perfectly conducting spheres using the CFDTD method.

The deformation of Faraday contours near the outside surface of a sphere is shown in Fig. 1. The H components represent the

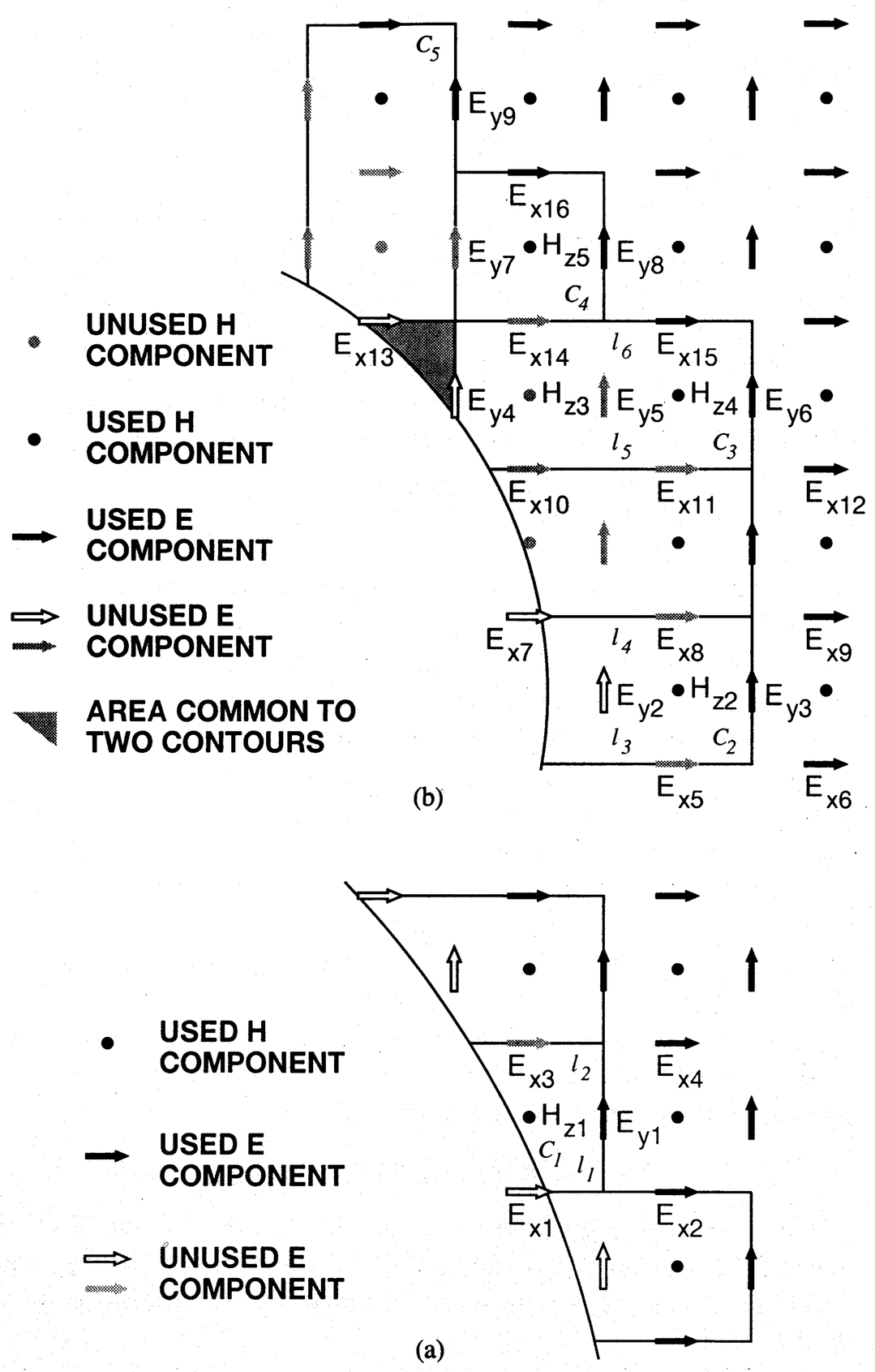

Fig. 1. CFDTD contours intersecting a perfectly conducting sphere. (a) Not near tangent to surface. (b) Almost tangent to surface.

average value of the magnetic field within the surface bounded by the deformed Faraday contour. The electric field $E_{\tan}$ at the object boundary is zero. Along the remaining straight portions of the contour, the electric field components are assumed to be constant along their respective contour segments. These electric field components are calculated using nondistorted rectangular Ampere contours, provided that the Ampere contours do not cross a media interface. The gray arrows and dots in the legend of Fig. 1 indicate which unused components would be used *if* this object were a (2-D) circular cylinder rather than a sphere. The white arrows indicate components which are unused in either case.

The integral along contour C_1, shown in Fig. 1(a), computes the magnetic field component H_{z1}. The difference equation for contour C_1 is

$$H_{z1}^{n+1/2}(i+1/2, j+1/2, k) = H_{z1}^{n-1/2}(i+1/2, j+1/2, k) \times \frac{\Delta t}{\mu_0 A_1} \cdot [E_{x4}^n(i+1\tfrac{1}{2}, j+1, k) \cdot l_2 - E_{y1}^n(i+1, j+\tfrac{1}{2}, k) \cdot \Delta y - E_{x2}^n(i+1\tfrac{1}{2}, j, k) \cdot l_1], \quad (5)$$

where A_1 is the area enclosed by C_1. Since component E_{x1} is inside the metal sphere it is not used to estimate the electric field along the contour side whose length is l_1. A nearest neighbor approximation for this field results in the use of the value of E_{x2}. The contour side containing the component E_{y1} is computed using E_{y1} and the length Δy. The electric field along the side whose length is l_2 can not use E_{x3} as its value, since the H_y component which lies underneath (in the z direction) E_{x3} is inside the sphere. Instead, the value of E_{x4} is used here. Note that if the media interface shown in Fig. 1 were for a two-dimensional geometry, such as a circular cylinder, this situation would not arise, as E_{x3} would not be dependent upon any H_y components.

The contours shown in Fig. 1(b) lie on a plane which has a perpendicular distance to the sphere's surface of only $1/2$ of a space increment. Therefore the surface of the sphere is close to this plane in the neighborhood of their intersection. This causes many of the field components near the media interface to be unuseable, as highlighted in white and gray in Fig. 1(b), because the field components needed to compute *them* are inside the sphere.

Contour C_2, displayed in Fig. 1(b), is used to compute the magnetic field component H_{z2}. The difference equation for contour C_2 is

$$H_{z2}^{n+1/2}(i+1/2, j+1/2, k) = H_{z2}^{n-1/2}(i+1/2, j+1/2, k) + \frac{\Delta t}{\mu_0 A_2} \cdot [E_{x9}^n(i+1\tfrac{1}{2}, j+1, k) \cdot l_4 - E_{y3}^n(i+1, j+\tfrac{1}{2}, k) \cdot \Delta y - E_{x6}^n(i+1\tfrac{1}{2}, j, k) \cdot l_3], \quad (6)$$

where A_2 is the area enclosed by C_2. The electric field along the side whose length is l_3 cannot use E_{x5} as its value, since the H_y component which is located underneath (in the z direction) E_{x5} is inside the sphere. Instead, the value of E_{x6} is used. A similar situation exists for the electric field along the side whose length is l_4: E_{x9} is used here instead of E_{x8}. The component E_{y2} is not used since at least one of the magnetic field components used for its calculation is inside the sphere.

Moving in a clockwise direction, contour C_3 contains the locations of E_{x10}, E_{x11}, E_{x13}, E_{x14}, E_{x15}, and E_{y6}. The gray electric field components cannot be computed since the H_y components underneath (in the z direction) them are inside the sphere. The component H_{z3} is not computed since all of the field components used for its computation are unuseable. H_{z4} represents the average magnetic field within contour C_3. The difference equation for contour C_3 is

$$H_{z4}^{n+1/2}(i+1/2, j+1/2, k) = H_{z4}^{n-1/2}(i+1/2, j+1/2, k) + \frac{\Delta t}{\mu_0 A_3} \cdot [E_{x15}^n(i+\tfrac{1}{2}, j+1, k) \cdot l_6 - E_{y6}^n(i+1, j+\tfrac{1}{2}, k) \cdot \Delta y - E_{x12}^n(i+1\tfrac{1}{2}, j, k) \cdot l_5], \quad (7)$$

where A_3 is the area enclosed by C_3. Electric field components E_{x10} and E_{x11} lie on a contour segment of length l_5 and the contour integration of this segment uses the value of E_{x12} here. The components E_{x13}, E_{x14}, and E_{x15} are positioned on a contour segment of length l_6 and the value of E_{x15} is used along its entire length. The gray shaded area is common to contours C_3 and C_5. The component E_{y4} is not used since at least one of the magnetic field components used for its calculation is inside the sphere. E_{y5} is unused since the H_y component which lies underneath it is situated inside the sphere.

Contour C_4, which is used to compute H_{z5}, is a square contour with side length equal to the space increment and area A_4 equal to $\Delta x\,\Delta y$. The difference equation for contour C_4 is

$$H_{z5}^{n+1/2}(i+1/2, j+1/2, k) = H_{z5}^{n-1/2}(i+1/2, j+1/2, k) + \frac{\Delta t}{\mu_0 A_4}\cdot[E_{y9}^{n}(i, j+1\tfrac{1}{2}, k)\cdot\Delta y + E_{x16}^{n}(i+\tfrac{1}{2}, j+1, k)\cdot\Delta x - E_{y8}^{n}(i+1, j+\tfrac{1}{2}, k)\cdot\Delta y - E_{x15}^{n}(i+1\tfrac{1}{2}, j, k)\cdot\Delta x]. \quad (8)$$

E_{x14} and E_{y7} are not useable since the H_y components which lie underneath them are positioned inside the sphere. The electric field value along their contour side are approximated with E_{x15} and E_{y9}, respectively.

IV. Numerical Results

In this section analytical and numerical data validations of the CFDTD method are presented. Near- and far-field steady-state validations are presented. The far-field comparisons are made with radar cross-section (RCS) data. Steady state data is extracted from the CFDTD and traditional FDTD codes by allowing the transient excitations to decay and then computing magnitudes and phases from the time domain data. The objects discussed here are perfectly conducting and illuminated with plane waves. The field approximations used in this investigation were stable for all the geometries modeled. The time increment used in the CFDTD simulations, $\delta t = \delta x/2c$, was identical to that used in the traditional FDTD runs.

A. Single Sphere

The first geometry considered is a moderately resolved, 1/20 wavelength cell size, $k_0 a = \pi$ sphere. Figs. 2, 3, and 4 are *near field* data comparisons between the CFDTD method and the series solution. The data presented is magnetic field data *near* the sphere's surface. The location of the field points are determined by their location in the cartesian FDTD mesh. This implies that distance from surface to a given field point is not constant from point to point. Their distance from the sphere's surface vary from almost touching to as much as 1.5 times Δx. Likewise, the computed series solution [14] is for near field values, *not* surface currents.

Figs. 2 and 3 show data comparisons of the x and y components, respectively, of the magnetic field in an H-plane cut. The angle $\phi = 0°$ represents the backscatter direction. Fig. 4 shows a comparison of the y component of the magnetic field in an E-plane cut. This cut is offset a half space cell, $1/2\Delta x$, from a vertically oriented great circle (dashed line). The angle $\alpha = 0°$ is

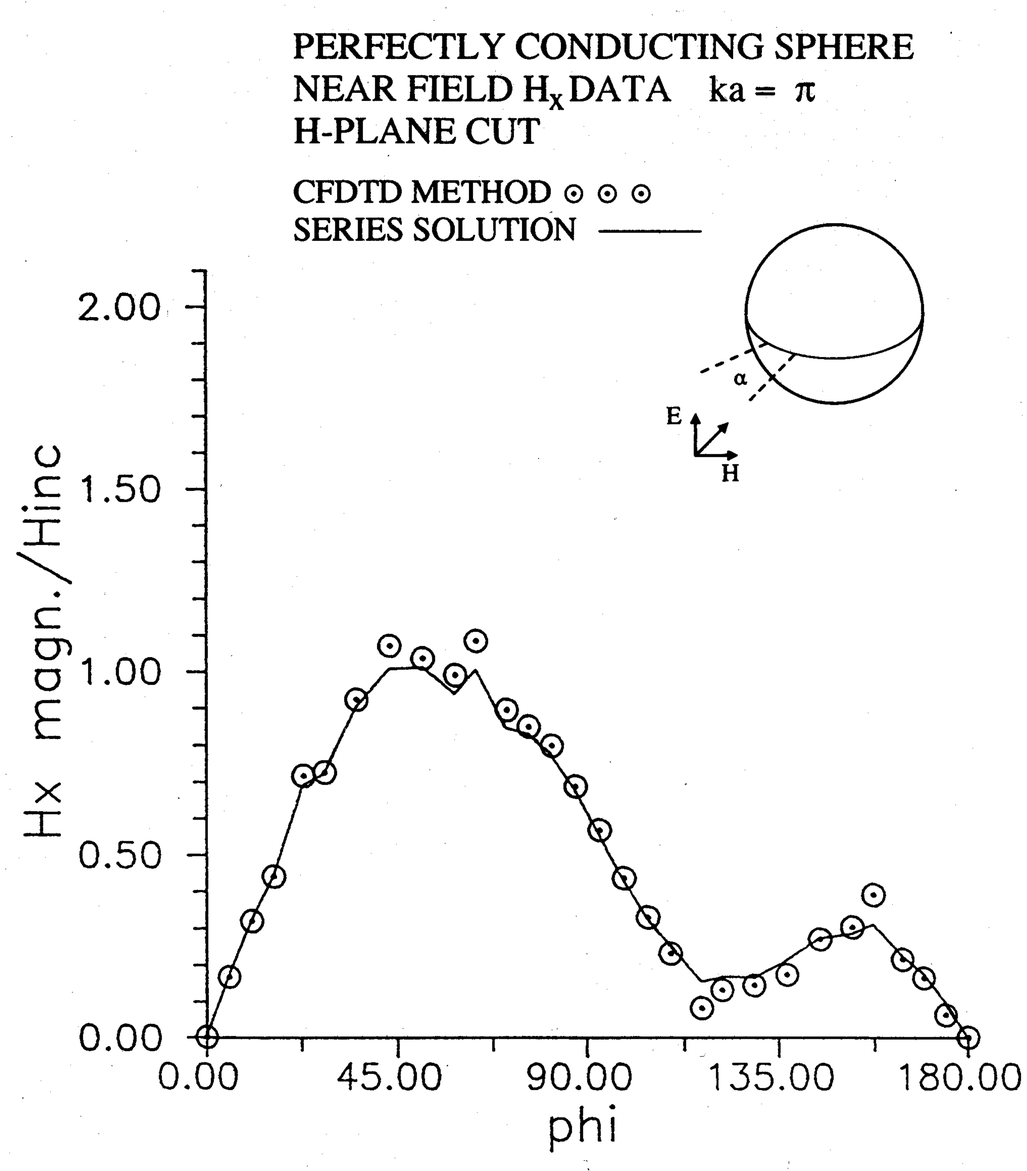

Fig. 2. H_x near field sphere data, H-plane cut.

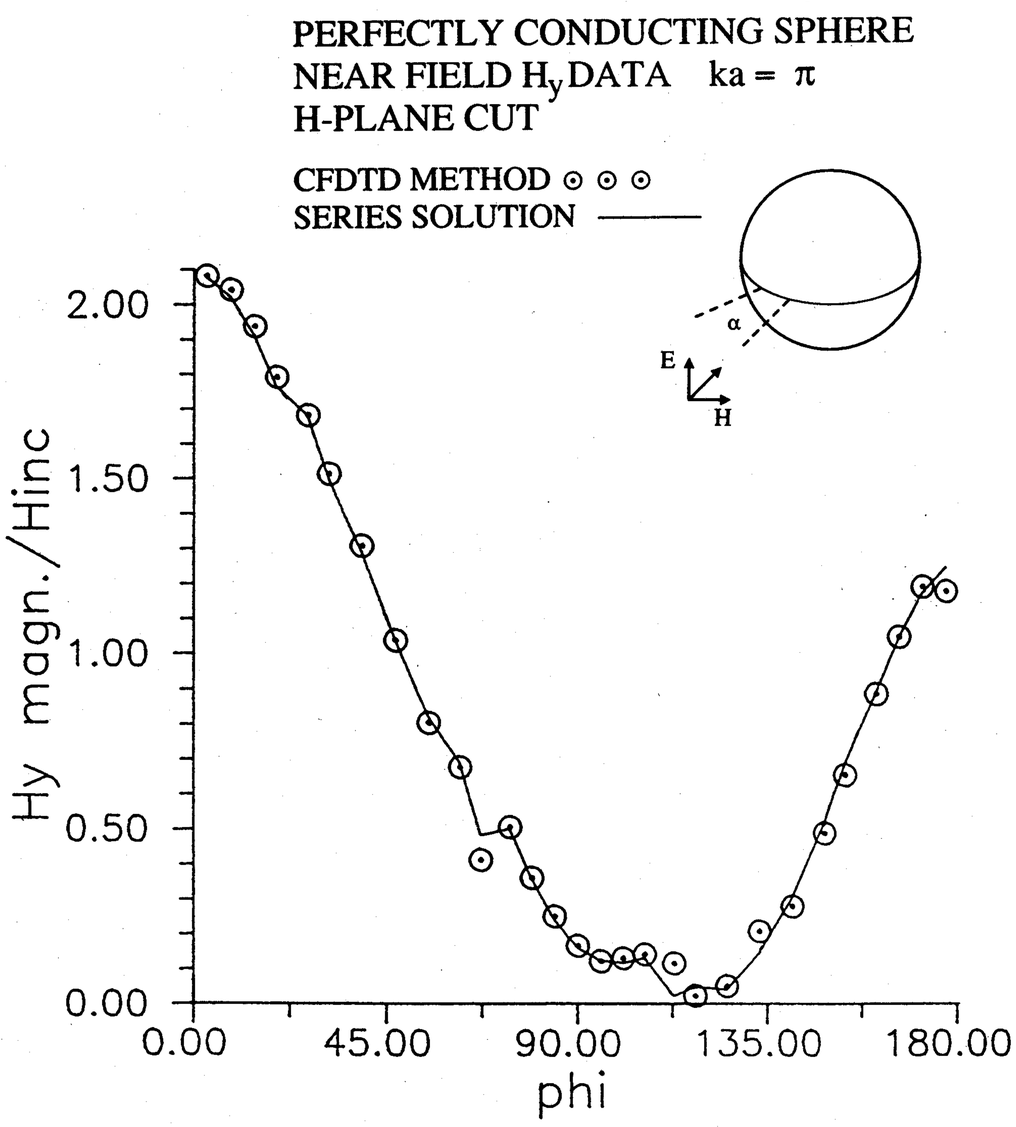

Fig. 3. H_y near field sphere data, H-plane cut.

the backscatter direction. As can be seen in the graphs, the CFDTD data shows excellent agreement with the series solution.

Figs. 5 and 6 display the E-plane and H-plane bistatic RCS of a $k_0 a = \pi$ sphere. The angle $\phi = 0°$ is the backscatter direction. Here, the CFDTD data is compared to the series solution and also the traditional FDTD derived data. These figures show that the CFDTD method is a significant improvement over the traditional FDTD method.

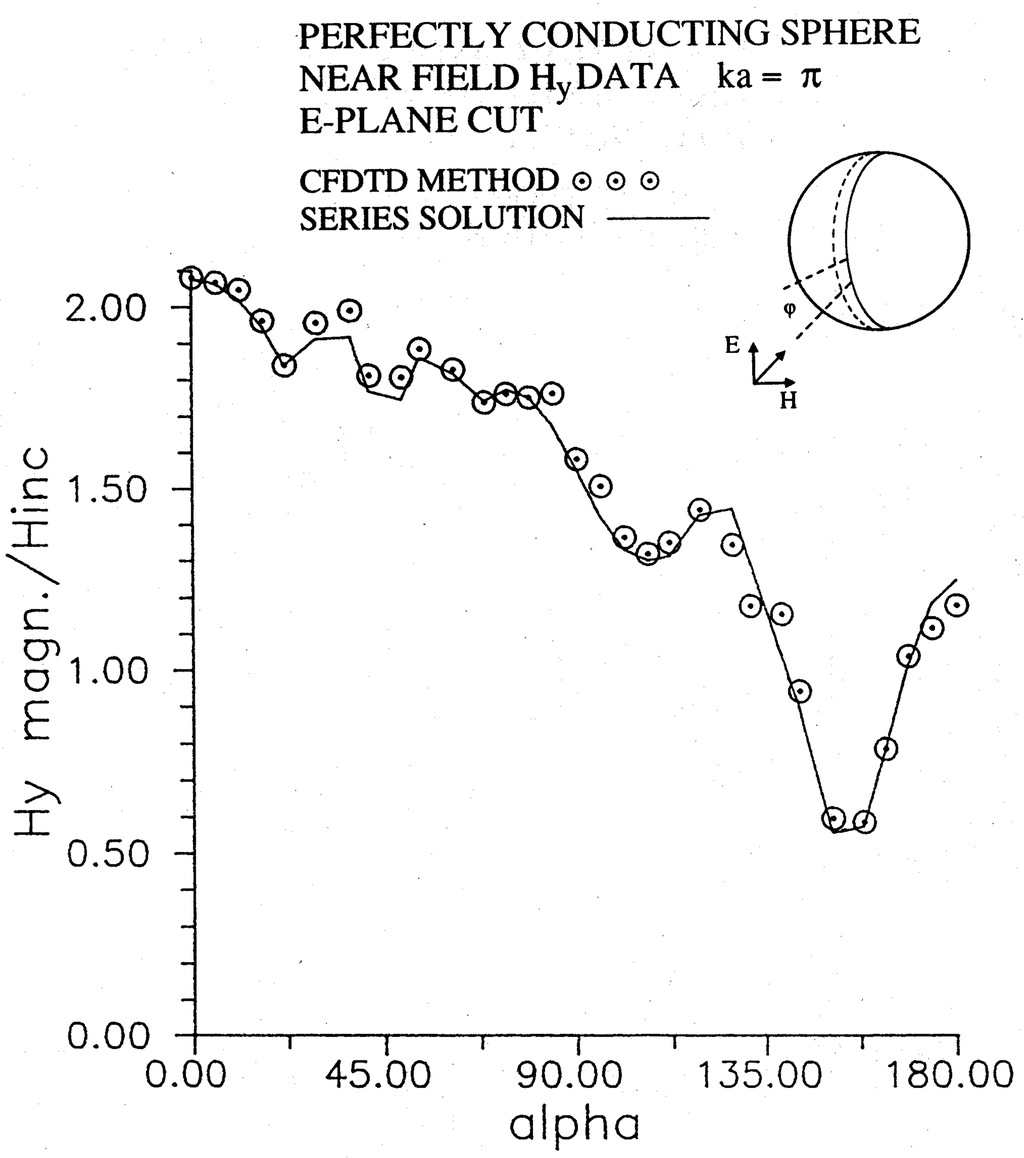

Fig. 4. H_y near field sphere data, offset E-plane cut.

Fig. 5. E-plane bistatic RCS of a sphere.

B. Double Sphere

The next examples are systems of two spheres. Two decades ago scattering from multiple spheres was investigated by Bruning [15], [16]. Our data comparisons are made to the generalized multipole technique (GMT) as reported by Ludwig [17].

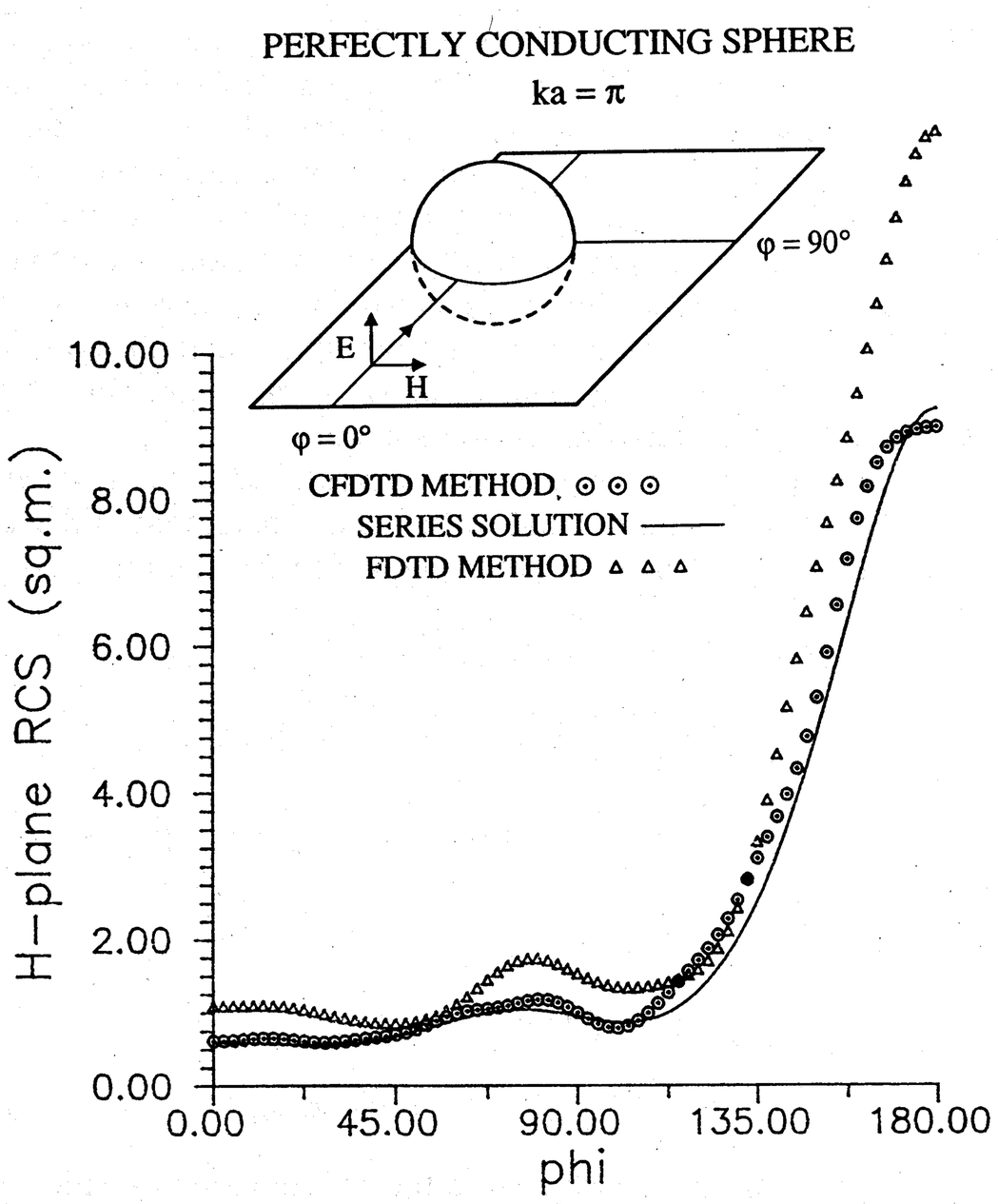

Fig. 6. H-plane bistatic RCS of a sphere.

The first geometry presented is a system of two $k_0a = \pi$ spheres whose centers are separated by two wavelengths. The CFDTD cell resolution is 1/20 wavelength. Fig. 7 displays the E-plane bistatic RCS of two spheres subjected to illumination along the axis defined by the spheres' centers. The angle $\phi = 0°$ is the backscatter direction. The CFDTD method agrees well with the GMT. The RCS data shown here has over 40 dB of dynamic range which compares favorably with previous FDTD results for a large T-shaped plate [1]. This figure also shows the relatively poor results obtained from modeling the two spheres with the traditional FDTD method. Fig. 8 shows the E-plane bistatic RCS of two spheres subjected to illumination 45° off the axis defined by the spheres' centers. The angle $\phi = 45°$ is the backscatter direction. Note the CFDTD method's ability to follow the complicated pattern of peaks and nulls.

The next geometry presented is a system of two $k_0\alpha = \pi$ spheres whose centers are separated by 1.25 wavelengths. The CFDTD cell resolution is 1/20 wavelength. Fig. 9 shows the E-plane bistatic RCS of two spheres subjected to illumination at 45° off the axis defined by the spheres' centers. The backscatter direction is 45°. The CFDTD method agrees well with the GMT. This figure also illustrates the relatively poor results obtained from modeling with the traditional FDTD method.

V. Computer Resource Comparisons

The time step requirements for the FDTD code and the CFDTD code depend upon the data desired from the algorithm, i.e., transient or steady state data, and the maximum linear

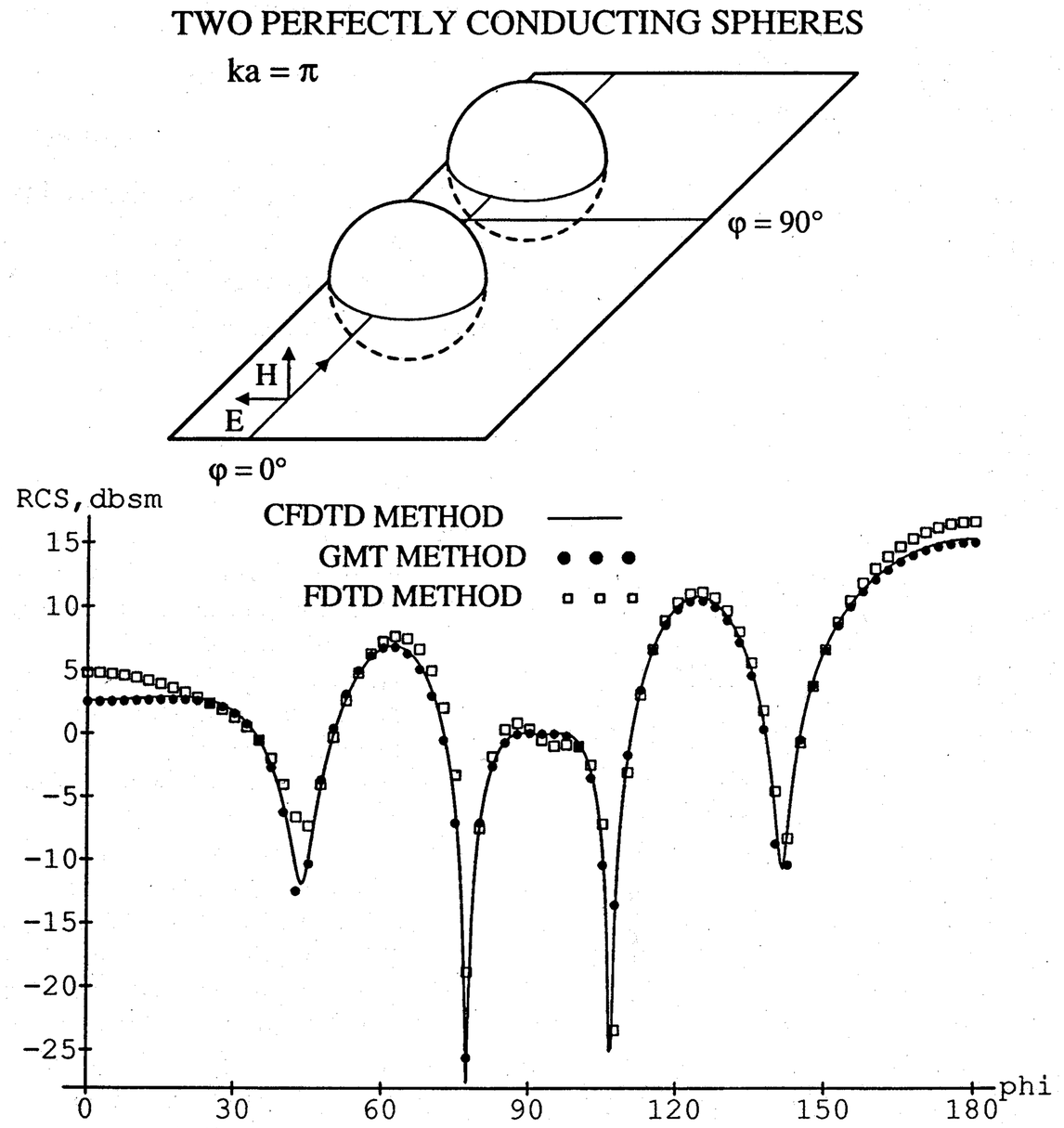

Fig. 7. Bistatic RCS of a system of two spheres, 2.0 wavelength center-to-center separation, axial incidence.

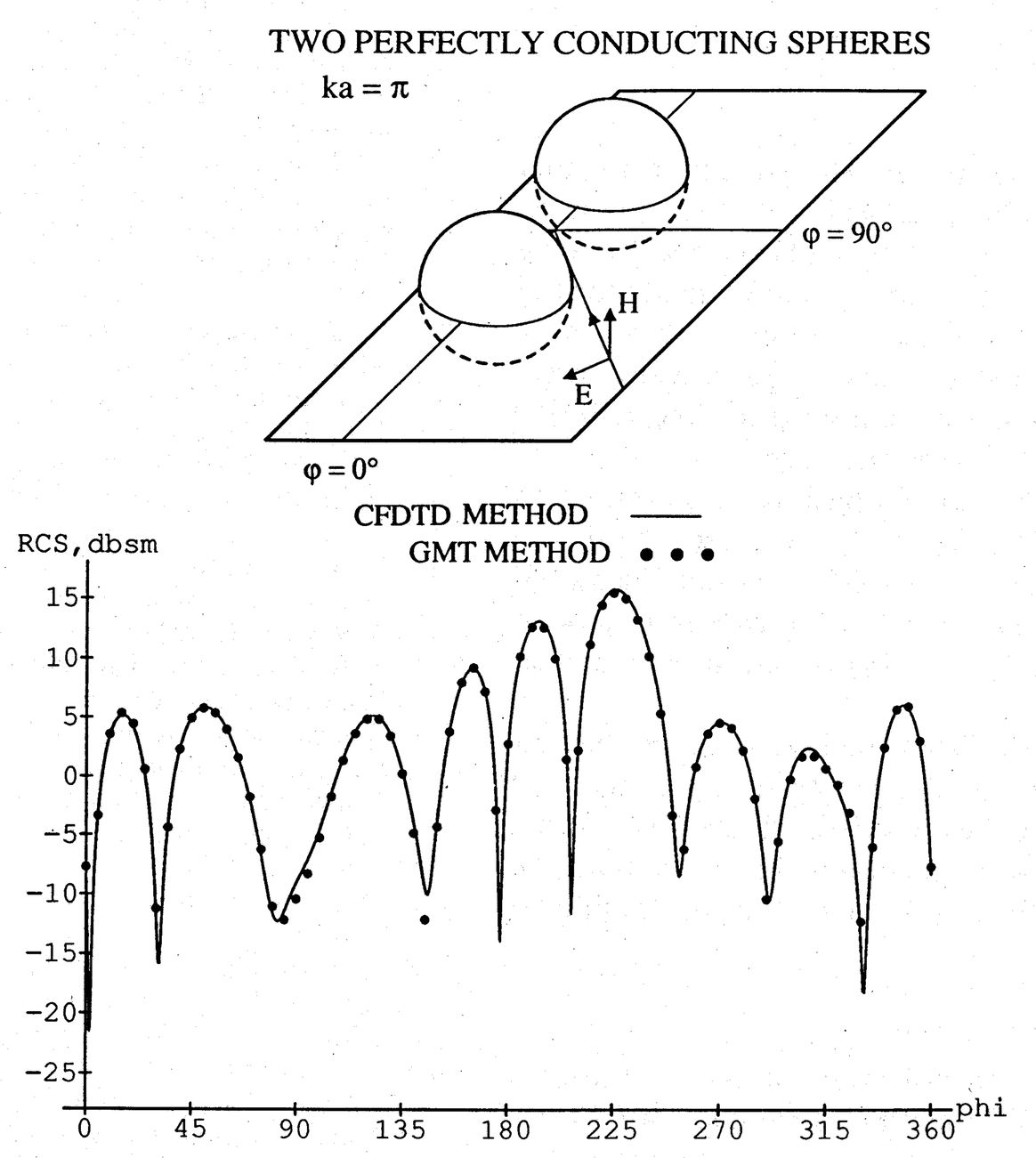

Fig. 8. Bistatic RCS of a system of two spheres, 2.0 wavelength center-to-center separation, 45° incidence.

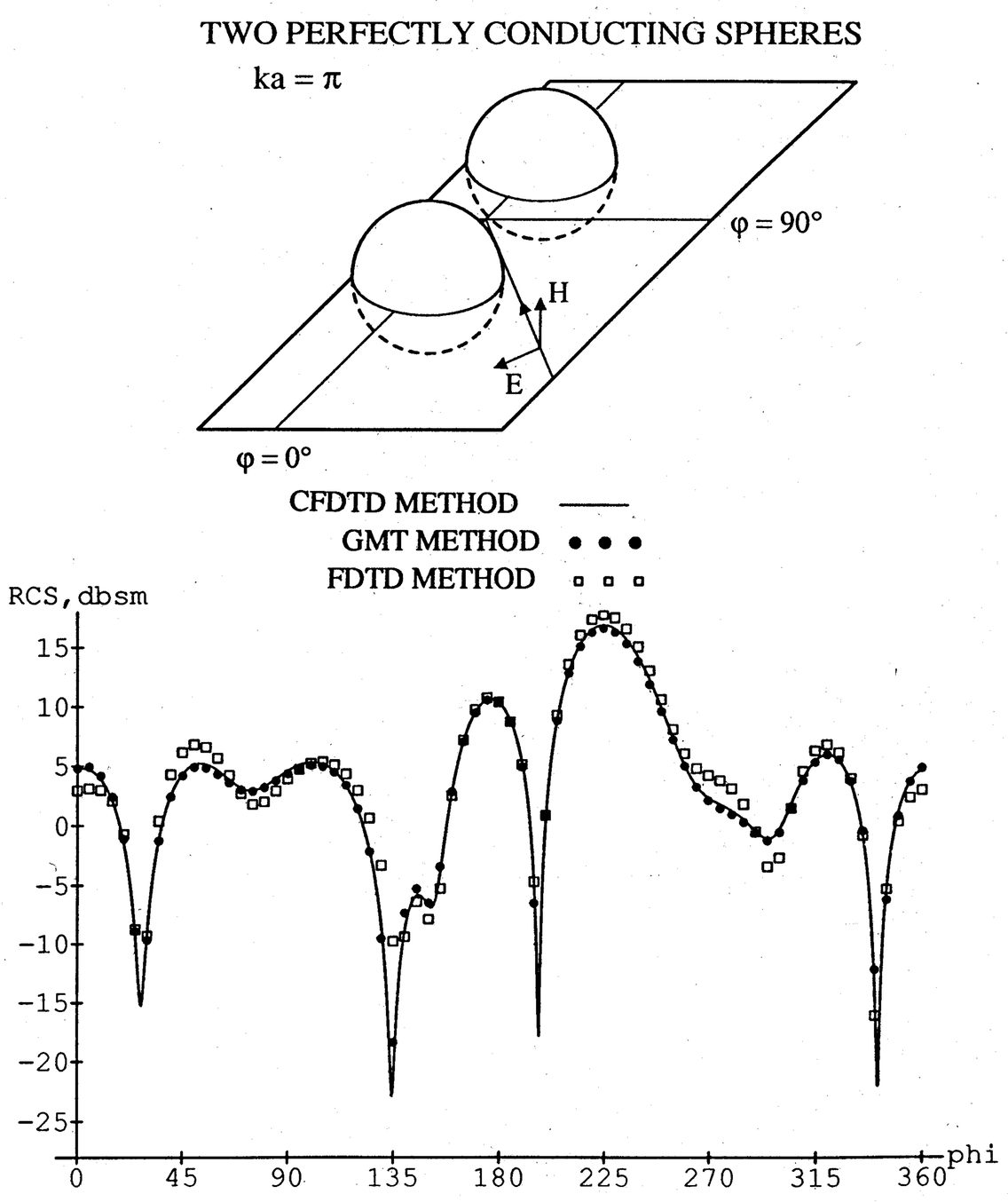

Fig. 9. Bistatic RCS of a system of two spheres, 1.25 wavelength center-to-center separation, 45° incidence.

dimension, L, of the scattering system. The computer memory demands of the traditional FDTD code scale with the volume L^3 of the computational lattice. Since the CFDTD code is only employed at media interfaces, the memory requirements for the nonrectangular contours scale with scatterer surface area. Therefore as the scattering system becomes electrically large, the increase in cost of obtaining a solution using the CFDTD method over using the FDTD method diminishes as $1/L$.

The number of field components (which is proportional to memory) needed for CFDTD computation increased by 0.24% as compared to FDTD computation. CFDTD run time increased by 3.9% over FDTD. These quantities are derived from modeling a single sphere in a $40 \times 40 \times 40$ lattice and two spheres in a $40 \times 40 \times 80$ lattice.

Mesh generation for the CFDTD method is more difficult than the FDTD method. Contour side lengths and areas as well as field approximations need to be considered. Experience with a primitive two-dimensional mesh generator indicates that the CFDTD mesh generation time is double that of traditional FDTD mesh generation.

VI. Conclusion

This paper introduced a generalization of the 3-D FDTD method, the 3-D contour FDTD method. Examples of CFDTD modeling of 3-D electromagnetic wave scattering were presented. The CFDTD method provided increased accuracy over the FDTD method when modeling the illumination of bodies with curved surfaces. The computer resources needs of the CFDTD method were shown to be negligibly greater than for the FDTD method.

Acknowledgment

The authors thank Evans Harrigan of Cray Research, Inc. for the use of the Cray YMPs used in some of the CFDTD and FDTD runs. We also thank Art Ludwig of General Research Corp. for the GMT validations.

References

[1] A. Taflove, "Review of the formulation and applications of the finite difference time-domain method for numerical modeling of electromagnetic wave interactions with arbitrary structures," *Wave Motion*, vol. 10, no. 6, 1988.

[2] A. C. Cangellaris and D. B. Wright, "Analysis of the numerical error caused by the stair-stepped approximation of a conducting boundary in FDTD simulations of electromagnetic phenomena," *IEEE Trans. Antennas Propagation*, vol. 39, pp. 1518–1525, Oct. 1991.

[3] T. G. Jurgens, A. Taflove, K. R. Umashankar, and T. G. Moore, "Finite difference time domain modeling of curved surfaces," *IEEE Trans. Antennas Propagation*, vol. 40, Apr. 1992.

[4] R. Holland, "Finite difference solution of Maxwell's equations in generalized nonorthogonal coordinates," *IEEE Trans. Nucl. Sci.*, vol. 30, pp. 4589–4591, Dec. 1983.

[5] M. A. Fusco, M. V. Smith, and L. W. Gordon, "A three dimensional FDTD algorithm in curvilinear coordinates," *IEEE Trans. Antennas Propagation*, vol. 39, pp. 1463–1471, Oct. 1991.

[6] D. S. Katz, M. J. Piket-May, A. Taflove, and K. R. Umashankar, "FDTD analysis of electromagnetic wave radiation from systems containing horn antennas," *IEEE Trans. Antennas Propagation*, vol. 39, pp. 1203–1212, Aug. 1991.

[7] A. Taflove, K. R. Umashankar, B. Beker, F. Harfoush, and K. S. Yee, "Detailed FD-TD analysis of electromagnetic fields penetrating narrow slots and lapped joints in thick conducting screens," *IEEE Trans. Antennas Propagation*, vol. 36, pp. 247–257, Feb. 1988.

[8] P. A. Tirkas and K. R. Demarest, "Modeling of thin dielectric structures using the finite difference time domain technique," *IEEE Trans. Antennas Propagation*, vol. 39, pp. 1338–1344, Sept. 1991.

[9] C. C. Shang and J. F. DeFord, "Modified Yee solutions in the AMOS wakefield code," in *Proceedings of the* 1990 *Linear Accelerator Conference* (Albuquerque, NM), pp. 378–380, Sept. 1990.

[10] T. G. Jurgens and F. A. Harfoush, "Conformal FDTD modelling of 3D wake fields," in *Proceedings of the* 14*th Biennial IEEE Particle Accelerator Conference* (San Francisco, CA), pp. 321–323, May 1991.

[11] F. A. Harfoush and T. G. Jurgens, "Visualization of wake fields in 3D," in *Proceedings of the* 14*th Biennial IEEE Particle Accelerator Conference* (San Francisco, CA), pp. 2512–2514, May 1991.

[12] K. S. Yee, "Numerical solution of initial boundary value problems involving Maxwell's equations in isotropic media," *IEEE Trans. Antennas Propagation*, vol. 14, pp. 302–307, May 1966.

[13] G. Mur, "Absorbing boundary conditions for the finite-difference approximation of time-domain electromagnetic field equations," *IEEE Trans. Electromagnet. Compat.*, vol. 23, pp. 377–382, Nov. 1981.

[14] D. E. Barrick, *Radar Cross Section Handbook*. New York: Plenum, 1970.

[15] J. H. Bruning and Y. T. Lo, "Multiple scattering of EM waves by spheres, Part I—multipole expansion and ray optical solution," *IEEE Trans. Antennas Propagation*, vol. 19, pp. 378–390, May 1971.

[16] J. H. Bruning and Y. T. Lo, "Multiple scattering of EM waves by spheres, Part II—numerical and experimental results," *IEEE Trans. Antennas Propagation*, vol. 19, pp. 391–398, May 1971.

[17] A. C. Ludwig, "Scattering by two and three spheres computed by the generalized multipole technique," *IEEE Trans. Antennas Propagation*, vol. 39, pp. 703–705, May 1991.